IJST, Transactions of Mechanical Engineering, Vol. 38, No. M1, pp 119-133
Printed in The Islamic Republic of Iran, 2014

ACTIVE VIBRATION SUPPRESSION AND MANEUVER CONTROL OF AN ORBITING SMART FLEXIBLE SATELLITE*

E. AZADI[1], S. A. FAZELZADEH[2], M. EGHTESAD[3] AND M. AZADI[4**]

[1,2,3]School of Mechanical Engineering, Shiraz University, Shiraz, I. R. of Iran
[4]Dept. of Mechanical Engineering, Science and Research Branch, Islamic Azad University, Fars, I. R. of Iran
Email: mazadi@shirazu.ac.ir

Abstract– In this paper, vibration suppression and control of a smart flexible satellite maneuvering in a circular orbit are studied. The satellite is considered as a rigid hub and two flexible appendages with PZT (lead zirconate titanate) layers attached on them as sensors and actuators. Flexible satellite governing equations of motion are obtained using Lagrange-Rayleigh-Ritz technique and assumed mode method; these dynamic equations of motion of the flexible satellite are nonlinear and coupled. A thorough look at the resulting equations reveals that the flexible satellite dynamics that include the appendage vibrations and its rigid maneuver occur in two different time scales. Therefore, the dynamics of the flexible satellite can be divided into two fast and slow subsystems using the singular perturbation theory. The slow and fast subsystems are associated with rigid maneuver and appendages vibrations, respectively. A hybrid controller is proposed which consists of an adaptive inverse dynamics for slow subsystem maneuvering control, and a Lyapunov based controller for vibration suppression of the fast subsystem. Use of adaptive controller allows us to cope with parameters uncertainty for the rigid motion of the system. Using the Lyapunov approach the stability of these hybrid controllers is studied. Finally, the whole system is simulated and the simulation results show the effective performance of the proposed hybrid controller.

Keywords– Smart flexible satellite, orbital maneuver, adaptive inverse dynamics control, singular perturbation theory, active vibration

1. INTRODUCTION

For several reasons a satellite must be able to re-orient and perform tracking maneuvers. These maneuvers will cause certain levels of vibrations to flexible appendages. Many researchers have studied dynamics and control of spacecrafts having space maneuvers [1-5].

Some researchers investigated the control of satellite maneuver and appendage vibration. Hu [6] designed an adaptive back stepping controller for flexible spacecraft attitude maneuver and elastic vibration control. This controller takes into consideration the bounds on angular velocity. A fault-tolerant adaptive back stepping sliding mode control scheme was developed for flexible spacecraft attitude maneuvering using redundant reaction wheels in the presence of parametric uncertainty disturbances and unknown faults by Jiang *et al* [7]. Erdong and Zhaowei [8] studied an attitude regulation control using passivity-based technique for maneuvering flexible spacecraft. In the above studies no smart materials were used to suppress the vibration of the spacecraft appendages.

Many studies have been conducted when smart materials and piezoelectric layers are used as sensors and actuators for active vibration suppression of spacecraft flexible appendages. Li and Bainum [9]

*Received by the editors May 4, 2013; Accepted October 8, 2013.
**Corresponding author

applied the so-called momentum exchange feedback control and distributed piezoelectric actuator technology for the vibration control of a flexible spacecraft; they considered satellite as a rigid hub with cantilever flexible beam appendage which could undergo a single axis rotation. Hu and Ma designed a generalized control scheme based on the variable structure output feedback and active vibration control techniques using piezoceramics attached on the panel for the large angle attitude maneuver control of flexible spacecraft [10]. Also, they studied the vibration control of flexible spacecraft during attitude maneuver. The variable structure output feedback control was used to determine the flywheel torque for maneuver control and piezoelectric materials for active vibration suppression [11]. Hu [12] proposed a generalized scheme based on the sliding mode and active vibration control techniques for a flexible spacecraft equipped with piezoelectric layers. He used a simplified model for the large angle attitude maneuver. Qiu *et al* [13] presented the theoretical analysis and experimental results of active vibration suppression of a smart flexible cantilever plate. To decouple the bending and torsional vibration for measuring and driving, gyroscope and PZT patches were used as sensors and actuators by utilizing optimal placement. Azadi *et al* [14] applied an adaptive-robust control scheme to control the maneuver of a flexible satellite while suppressing the vibrations of the appendages. They used the piezoelectric layers as actuators. Also, Azadi [15] used a robust passivity based control to control the maneuver of the satellite and suppress the appendages vibration.

In some researches the spacecrafts are considered in a circular orbit, in order to control their orbital maneuver and vibration suppression, the effects of their motion in the orbit have to be considered. Singh and Zhang [16] designed an adaptive control system for a single axis rotational maneuver and vibration suppression of an orbiting spacecraft with flexible appendages. For synthesis of the control law, only the pitch angle was used for feedback. Hui *et al* [17] considered the control of entire-formation maneuvering in low-thrust Earth-orbiting spacecraft formation flying (SFF). In their study each spacecraft was modeled as a point mass. Maganti and Singh [18] designed a simple adaptive control system for the rotational maneuver around one axis of an orbiting spacecraft with flexible appendage. They considered a linear approximated model by ignoring the orbiting effects and other nonlinearities. Dong *et al* [19] applied an adaptive fuzzy sliding mode controller for the networked control systems with nonlinear and uncertain parameters during the flexible spacecraft slew maneuver. The spacecraft moved in a circular orbit. They reduced and decomposed the dynamics equations of the spacecraft into three single-input subsystems. Hu *et al*. [20] investigated a robust nonlinear control design under the constraints of assigned velocity and actuator torque for attitude stabilization of a rigid spacecraft. In these studies, vibration suppression is not directly considered; so, there is no use of smart materials for stabilization of vibration of the appendages.

In this paper the nonlinear governing equations of motion of a flexible satellite with piezoelectric layers are derived and no simplification or reduction is applied to these equations. The satellite is considered as a rigid hub with two flexible appendages with attached piezoelectric layers. The spacecraft rotates in circular orbit with constant speed and has pitch angle rotation maneuver. The piezoelectric layers are used as actuator and sensor to suppress vibration of panels. Also, the hybrid adaptive inverse dynamics/Lyapunov control is designed to control spacecraft maneuver and vibration suppression of panels together. This adaptive control scheme is robust against parameter uncertainties. Finally, the simulation results show the effectiveness and performance of controller.

2. SYSTEM DYNAMICS

a) Governing equations

In this study we consider a spacecraft with a rigid hub and two flexible appendages. The piezoelectric layers are attached to the appendages (see Fig. 1). Each appendage is proposed as a cantilever beam with

length L, width b, thickness t_a, density ρ, Young's modulus E and momentum of inertia *I*. The thickness of each piezoelectric layers is t_p, the density is ρ_p, Young's modulus is E_p, width b and the equivalent piezoelectric coefficient is shown by e_{31}. The lateral deflection of each point of the *i*th appendage is denoted by $w_i(x)$. Each pair of piezoelectric layers is attached on opposite sides of the appendage from x_{1n} to x_{2n} ($n=1,2,...,N$), where N is the number of piezoelectric layers. XYZ is an earth-center inertial reference frame such that XZ is the orbit plane. The origins of the coordinate frames $x_i y_i z_i$ ($i=1,2$) are attached to the hub center. We consider the spacecraft moving in a circular orbit with constant angular speed Ω; it also has a rotational maneuver around its z_1 axis with angular speed of $\dot{\psi}$, see Fig. 1.

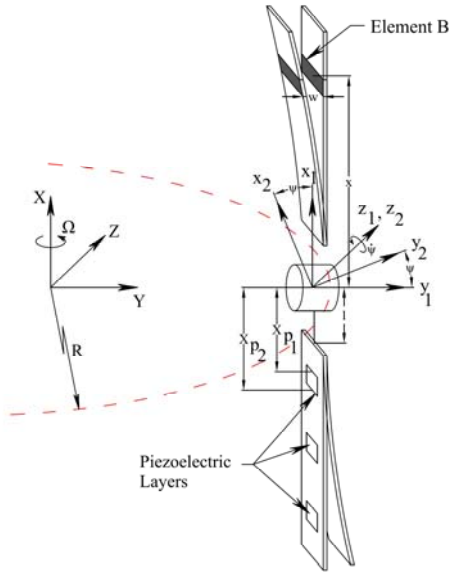

Fig. 1. Schematic view of the spacecraft in orbit and its coordinates

The velocity of an appendage element v_B can be determined by using the following equation:

$$v_B = v_A + v_{B/A} + \omega \times r_{B/A} \tag{1}$$

v_A is the hub velocity and $v_{B/A}$ is relative velocity of point B with respect to the rigid hub. ω is the vector of hub's angular velocity, $r_{B/A}$ is the position vector. v_A, $v_{B/A}$, ω and $r_{B/A}$ are obtained by the following equations:

$$v_A = R\Omega \hat{K},\ v_{B/A} = \dot{w}\,\hat{j}_2,\ \omega = \dot{\psi}\,\hat{k}_1 + \Omega \hat{I},\ r_{B/A} = x\,\hat{i}_2 + w\,\hat{j}_2 \tag{2}$$

where ($\dot{}$) means $\frac{d}{dt}(\,)$. Now one can obtain velocity of point B as:

$$\begin{aligned} v_B^2 = {} & \dot{w}^2 + 2\dot{w}\dot{\psi}x + \dot{\psi}^2 x^2 + \dot{\psi}^2 w^2 + R^2\Omega^2 + 2R\Omega^2 w\cos\psi - 2R\Omega^2 x\sin\psi + \\ & \Omega^2 w^2\cos^2\psi + \Omega^2 x^2\sin^2\psi - 2\Omega^2 wx\cos\psi\sin\psi \end{aligned} \tag{3}$$

The kinetic energy of the panels, hub and piezoelectric layers can be obtained as:

$$\begin{aligned} T = T_{app} + T_H + T_{PZT} = {} & \frac{1}{2}\rho t_a b\sum_{a=1}^{2}\int_{app_a} v_B^2 dx + \\ & (\frac{1}{2}M_h R^2\Omega^2 + \frac{1}{2}I_{h_z}\dot{\psi}^2 + \frac{1}{2}I_{h_y}\Omega^2\sin^2\psi + \frac{1}{2}I_{h_x}\Omega^2\cos^2\psi) + \frac{1}{2}\rho_p t_p b\sum_{a=1}^{2}\sum_{n=1}^{N_a}\int_{PZT_k} v_B^2 dx \end{aligned} \tag{4}$$

where M_h is hub's mass, I_{h_x}, I_{h_y}, and I_{h_z} are hub moments of inertia around x_2, y_2, and z_2 axes, respectively. N_a is the number of piezoelectric layers on ath appendage.
We consider each appendage as a Euler- Bernoulli beam, so the displacement field of the beam can be written as [21]:

$$u_{a\,x}(x,t) = -y\frac{\partial w_a(x,t)}{\partial x} \qquad a = 1,2 \tag{5}$$

where $w_a(x,t)$ and $u_{a\,x}(x,t)$ are the displacements in y direction and longitudinal x direction of the ith appendage in $x_2 y_2 z_2$ coordinate frame, respectively. The strain ε_x and stress σ_x in the appendages are as follows [21]:

$$\varepsilon_x = -y\frac{\partial^2 w_a(x,t)}{\partial x^2}, \qquad \sigma_x = -Ey\frac{\partial^2 w_a(x,t)}{\partial x^2}, \qquad a = 1,2 \tag{6}$$

The stress in piezoelectric layers can be expressed as [22], [23]:

$$\sigma_{x_{p_n}} = -E_{p_n} y\frac{\partial^2 w_{p_n}}{\partial x^2} - e_{31n}E_{z_n} \qquad n = 1\ldots N \tag{7}$$

where the subscript p_n represents the nth piezoelectric layer and $E_{z_n} = v_n / h_{p_n}$ $(n = 1\ldots N)$ is the electric field in the nth piezoelectric layer. The first and second terms on the right hand side of Eq. (7) are the stresses due to the mechanical and electrical effects of the piezoelectric layers, respectively.
On the other hand, the potential energy of the panel and piezoelectric layers are:

$$\begin{aligned} U_{app} &= \frac{1}{2}\sum_{a=1}^{2}\int_{app_a} Ey^2\left(\frac{\partial^2 w_a}{\partial x^2}\right)^2 dv \\ U_{PZT} &= \frac{1}{2}\sum_{n=1}^{N}\int_{PZT_n} E_{p_n} y^2\left(\frac{\partial^2 w_{p_n}}{\partial x^2}\right)^2 dv + \sum_{n=1}^{N}\int_{PZT_n} ye_{31}E_{z_n}\frac{\partial^2 w_{p_n}}{\partial x^2} dv \\ &\quad + \frac{1}{2}\sum_{n=1}^{N}\int_{PZT_n} E_{z_n} d_n dv \end{aligned} \tag{8}$$

where y is the axis perpendicular to the piezoelectric surface, and d_n is the electric displacement for the nth patch. The electric displacement is:

$$d_n = \varepsilon_{p_n}\frac{v_n}{t_p} \tag{9}$$

wherein ε_{p_n} is the dielectric constant of the piezoelectric material which forms the nth patch. The last term in Eq. (8) is the electric energy stored in the piezoelectric material.

The equation of motion and boundary conditions will be derived using Lagrange's method which may be expressed as: [24], [25]

$$\frac{d}{dt}\left(\frac{\partial T}{\partial \dot{\zeta}}\right) - \frac{\partial T}{\partial \zeta} + \frac{\partial U}{\partial \zeta} = Q \tag{10}$$

where $U = U_{app} + U_{PZT}$ and $T = T_{app} + T_{PZT} + T_h$ are strain energy and kinetic energy, respectively, and Q is the generalized force. ζ refers to the vector of generalized coordinates consisting of satellite rotation angles and two appendages vibration coordinates.

b) Rayleigh–Ritz formulation

Due to the intricacy of the governing equations, their solution may be achieved by an approximate solution procedure. To this end, w_j can be represented by a series of trial shape functions, ϕ_i^j, satisfying the boundary conditions, of which, each is multiplied by a time dependent generalized coordinate, q_i^j, that is,

$$\begin{aligned} & w_j(x,t) = \sum_i \varphi_i^j q_i^j = (\mathbf{\Phi}^j)^T \mathbf{q}^j \qquad j = 1,2 \\ & \mathbf{\Phi} = [(\mathbf{\Phi}^1)^T \quad (\mathbf{\Phi}^2)^T]^T \\ & \mathbf{q} = [(\mathbf{q}^1)^T \quad (\mathbf{q}^2)^T]^T \end{aligned} \tag{11}$$

where $\mathbf{\Phi}^j$ and $\mathbf{q}^j$ are the vectors of assumed mode shapes and generalized coordinates of the j th appendage, respectively.

The terms in right hand side of Eq. (4) are kinetic energy of panels, hub and piezoelectric layers denoted by T_{app}, T_H and T_{PZT}, respectively.

$$\begin{aligned} T_{app} = & \frac{1}{2}\rho t_a b \sum_{a=1}^{2} \{ \sum_i \sum_j (\dot{q}_i^a \dot{q}_j^a \int_{app_a} \varphi_i^a \varphi_j^a dx) + \dot{\psi}^2 \int_{app_a} x^2 dx + \dot{\psi}^2 \sum_i \sum_j (q_i^a q_j^a \int_{app_a} \varphi_i^a \varphi_j^a dx) \\ & + 2\dot{\psi} \sum_i (\dot{q}_i^a \int_{app_a} \varphi_i^a x dx) + R^2 \Omega^2 \int_{app_a} dx + \Omega^2 \cos^2\psi \sum_i \sum_j (q_i^a q_j^a \int_{app_a} \varphi_i^a \varphi_j^a dx) \\ & + \Omega^2 \sin^2\psi \int_{app_a} x^2 dx \\ & + 2R\Omega^2 \cos\psi \sum_i q_i^a \int_{app_a} \varphi_i^a dx - 2R\Omega^2 \sin\psi \int_{app_a} x dx - 2\Omega^2 \sin\psi \cos\psi \sum_i (q_i^a \int_{app_a} \varphi_i^a x dx) \} \end{aligned} \tag{12}$$

where q_i^a is i th component of a th appendage and T_H is:

$$T_H = \frac{1}{2} M_h R^2 \Omega^2 + \frac{1}{2} I_{h_z} \dot{\psi}^2 + \frac{1}{2} I_{h_y} \Omega^2 \sin^2\psi + \frac{1}{2} I_{h_x} \Omega^2 \cos^2\psi \tag{13}$$

and

$$\begin{aligned} T_{PZT} = & \frac{1}{2}\rho_p t_p b \sum_{a=1}^{2} \sum_{n=1}^{N_a} \{ \sum_i \sum_j (\dot{q}_i^a \dot{q}_j^a \int_{PZT_n^a} \varphi_i^a \varphi_j^a dx) + \dot{\psi} \int_{PZT_n^a} x^2 dx + \dot{\psi}^2 \sum_i \sum_j (q_i^a q_j^a \int_{PZT_n^a} \varphi_i^a \varphi_j^a dx) \\ & + 2\dot{\psi} \sum_i (\dot{q}_i^a \int_{PZT_n^a} \varphi_i^a x dx) + R^2 \Omega^2 \int_{PZT_n^a} dx + \Omega^2 \cos^2\psi \sum_i \sum_j (q_i^a q_j^a \int_{PZT_n^a} \varphi_i^a \varphi_j^a dx) \\ & + \Omega^2 \sin^2\psi \int_{PZT_n^a} x^2 dx + 2R\Omega^2 \cos\psi \sum_i q_i^a \int_{PZT_n^a} \varphi_i^a dx \\ & - 2R\Omega^2 \sin\psi \int_{PZT_n^a} x dx - 2\Omega^2 \sin\psi \cos\psi \sum_i (q_i^a \int_{PZT_n^a} \varphi_i^a x dx) \} \end{aligned} \tag{14}$$

Using Eq. (10) and applying the Rayleigh-Ritz procedure on the governing equations, the following set of ordinary differential equations is obtained:

$$\begin{bmatrix} M_{\psi\psi} & M_{\psi q} \\ M_{q\psi} & M_{qq} \end{bmatrix} \begin{Bmatrix} \ddot{\psi} \\ \ddot{\mathbf{q}} \end{Bmatrix} + \begin{bmatrix} C_{\psi\psi} & C_{\psi q} \\ C_{q\psi} & C_{qq} \end{bmatrix} \begin{Bmatrix} \dot{\psi} \\ \dot{\mathbf{q}} \end{Bmatrix} + \begin{bmatrix} 0 & 0 \\ 0 & K_{qq} \end{bmatrix} \begin{Bmatrix} \psi \\ \mathbf{q} \end{Bmatrix} + \begin{Bmatrix} K_{H_\psi} \\ K_{H_q} \end{Bmatrix} = \begin{Bmatrix} \boldsymbol{\tau} \\ -K_{p_{elastelect_a}} \boldsymbol{v_a} \end{Bmatrix} \tag{15}$$

$$\boldsymbol{v}_s = -K^{-1}_{p_{elect}} K^T_{p_{elastelect_s}} \mathbf{q}$$

where $\mathbf{q} = [(\mathbf{q}^1)^T \quad (\mathbf{q}^2)^T]^T$ and $\boldsymbol{\tau}$ is the control torque. $\boldsymbol{v}_a$ and $\boldsymbol{v}_s$ are the vectors of the actuator and sensor voltages, respectively. The elements of the mass matrix in Eq. (15) are:

$$\begin{aligned}(M_{\psi\psi}) = \rho b t_a \sum_{a=1}^{2}\{\int_{app_a} x^2 dx + \sum_i \sum_j q_i^a q_j^a \int_{app_a} \varphi_i^a \varphi_j^a dx\} \\ + \rho_p b t_p \sum_{a=1}^{2}\sum_{n=1}^{N_a}\{\int_{PZT_n^a} x^2 dx + \sum_i \sum_j q_i^a q_j^a \int_{PZT_n^a} \varphi_i^a \varphi_j^a dx\} + I_{h_z}\end{aligned} \tag{16}$$

$$(M_{\psi q})_{ij} = (M_{q\psi})_{ji} = \rho b t_a \sum_{a=1}^{2} \int_{app_a} \varphi_i^a x dx + \rho_p b t_p \sum_{a=1}^{2}\sum_{n=1}^{N_a} \int_{PZT_n^a} \varphi_i^a x dx \tag{17}$$

and

$$(M_{qq})_{ij} = \rho b t_a \sum_{a=1}^{2} \int_{app_a} \varphi_i^a \varphi_j^a dx + \rho_p b t_p \sum_{a=1}^{2}\sum_{n=1}^{N_a} \int_{app_n^a} \varphi_i^a \varphi_j^a dx \tag{18}$$

The matrix of Coriolis and centrifugal effects is defined as [26]:

$$\begin{aligned} C_{ij} &= \sum_{k=1}^{N} c_{ijk} \dot{\zeta}_k \\ \zeta &= [\psi \quad \mathbf{q}^T]^T \end{aligned} \tag{19}$$

where

$$c_{ijk} = \frac{1}{2}\left(\frac{\partial [M]_{ij}}{\partial \zeta_k} + \frac{\partial [M]_{ik}}{\partial \zeta_j} - \frac{\partial [M]_{jk}}{\partial \zeta_i}\right) \tag{20}$$

and

$$M = \begin{bmatrix} (M_{\psi\psi})_{1\times 1} & (M_{\psi q})_{1\times N} \\ (M_{q\psi})_{N\times 1} & (M_{qq})_{N\times N} \end{bmatrix} \tag{21}$$

is the mass matrix. The stiffness matrix is $K_{qq} = diag(K_{qq_1}, K_{qq_2})$ and

$$\begin{aligned} K_{qq_i} = \int_{app_a} EI \frac{\partial^2 \boldsymbol{\Phi}^i(x)}{\partial x^2} \frac{\partial^2 (\boldsymbol{\Phi}^i(x))^T}{\partial x^2} dx + \\ \sum_{n=1}^{N_a} \int_{PZT_n^a} E_p I_p \frac{\partial^2 \boldsymbol{\Phi}^i(x)}{\partial x^2} \frac{\partial^2 (\boldsymbol{\Phi}^i(x))^T}{\partial x^2} dx \end{aligned} \tag{22}$$

where $I_p = t_a b t_p \left(\frac{t_a}{2} + t_p\right)$ is the moment of inertia of each piezoelectric layer.

$K_{p_{elastelect_a}}$ and $K_{p_{elastelect_s}}$ in Eq. (15) are the matrices of the elastic-electric effect of the piezoelectric actuator and sensor layers:

$$K_{p_{elastelect_a}} = \begin{bmatrix} K^1_{p_{elastelect_a}} & 0 \\ 0 & K^2_{p_{elastelect_a}} \end{bmatrix},\ K^T_{p_{elastelect_s}} = \begin{bmatrix} K^1_{p_{elastelect_s}} & 0 \\ 0 & K^2_{p_{elastelect_s}} \end{bmatrix}^T \tag{23}$$

where 0 is the zero matrix and

$$K^i_{p_{elastelect_a}} \text{ or } K^i_{p_{elastelect_s}} = \begin{bmatrix} K^i_{pee_1} & K^i_{pee_2} & \cdots & K^i_{pee_{N_i}} \end{bmatrix} \tag{24}$$

herein $K^i_{pee_j}$ is the vector of the *j*th column of the elastic-electric matrix and is defined as

$$K^i_{pee_j} = \frac{e_{31j}}{t_p} \int_{PZT^i_j} y \frac{\partial^2 \mathbf{\Phi}^i}{\partial x^2} dv \tag{25}$$

$K_{p_{elect}}$ is the capacitance matrix of the piezoelectric patches

$$K_{p_{elect}} = \sum_{n=1}^{N} \int_{PZT_n} \varepsilon_{p_n} P_n P_n^T dv \tag{26}$$

where the $N \times 1$ vector P_n has zero entries, except for entry *n* which is equal to $1/t_p$.

The vectors K_{H_θ} and K_{H_q} in Eq. (15) are the effects of moving spacecraft in the orbit:

$$\begin{aligned}(K_{H_\psi})_i &= \rho b t_a \sum_{a=1}^{2} \{\Omega^2 \sin\psi \cos\psi \sum_i \sum_j (q_i^a q_j^a \int_{app_a} \varphi_i^a \varphi_j^a dx) - \Omega^2 \sin\psi \cos\psi \int_{app_a} x^2 dx \\ &+ R\Omega^2 \sin\psi \sum_i (q_i^a \int_{app_a} \varphi_i^a dx) + R\Omega^2 \cos\psi \int_{app_a} x dx + \Omega^2 \cos(2\psi) \sum_i (q_i^a \int_{app_a} \varphi_i^a x dx)\} \\ &+ \rho_p b t_p \sum_{a=1}^{2} \sum_{n=1}^{N} \{\Omega^2 \sin\psi \cos\psi \sum_i \sum_j (q_i^a q_j^a \int_{PZT_n^a} \varphi_i^a \varphi_j^a dx) - \Omega^2 \sin\psi \cos\psi \int_{PZT_n^a} x^2 dx \\ &+ R\Omega^2 \sin\psi \sum_i (q_i^a \int_{PZT_n^a} \varphi_i^a dx) + R\Omega^2 \cos\psi \int_{PZT_n^a} x dx + \Omega^2 \cos(2\psi) \sum_i (q_i^a \int_{PZT_n^a} \varphi_i^a x dx)\} \\ &+ I_{h_y} \Omega^2 \sin\psi \cos\psi - I_{h_x} \Omega^2 \sin\psi \cos\psi\end{aligned} \tag{27}$$

and

$$\begin{aligned}(K_{H_q})_i &= \rho b t_a \sum_{a=1}^{2} \{-\Omega^2 \cos^2\psi \sum_j (q_j^a \int_{app_a} \varphi_i^a \varphi_j^a dx) - R\Omega^2 \cos\psi \int_{app_a} \varphi_i^a dx \\ &+ \Omega^2 \sin\psi \cos\psi \int_{app_a} \varphi_i^a x dx\} + \rho_p b t_p \sum_{a=1}^{2} \sum_{n=1}^{N} \{-\Omega^2 \cos^2\psi \sum_j (q_j^a \int_{PZT_n^a} \varphi_i^a \varphi_j^a dx) \\ &- R\Omega^2 \cos\psi \int_{PZT_n^a} \varphi_i^a dx + \Omega^2 \sin\psi \cos\psi \int_{PZT_n^a} \varphi_i^a x dx\}\end{aligned} \tag{28}$$

3. HYBRID CONTROL SYSTEM DESIGN

The governing equations of motion of the system are decoupled into fast and slow subsystems by using singular perturbation method. A hybrid control strategy that consists of an adaptive inverse dynamics controller for maneuver attitude control (slow subsystem) and a Lyapunov-based controller for suppression of vibration of appendages (fast subsystem) is proposed to control both fast and slow subsystems.

a) Decomposition of the equations of motion by the singular perturbation theory

Singular perturbations cause a multi-time-scale behavior of dynamic systems characterized by the presence of both slow and fast transients in the system response to external stimuli. After dividing system into two fast and slow subsystems, a hybrid controller can be applied to them. For applying singular perturbation technique a state should be multiplied by a small positive parameter called perturbation parameter [27]. The magnitude of the elements of the stiffness matrix K_{qq} is very large in comparison to the other coefficient in Eq. (15) [27], therefore, the singular perturbation parameter ε and a new variable *z* may be defined as

$$\begin{aligned} [K_{qq}]\{\mathbf{q}\} &= k_m[\overline{K}_{qq}]\{\mathbf{q}\} = \{z\} \\ [\overline{K}_{qq}]\{\mathbf{q}\} &= \varepsilon^2\{z\} \end{aligned} \tag{29}$$

where k_m is the largest coefficient of the stiffness matrix, K_{qq}, ε is the singular perturbation parameter 27], and $\varepsilon^2 = 1/k_m$. It can be shown that $O(K_{p_{elastelect_a}}) = O(\varepsilon)$; therefore, $K_{p_{elastelect_a}}$ matrix can be written as

$$K_{p_{elastelect_a}} = \varepsilon\overline{K}_{p_{elastelect_a}} \tag{30}$$

Substituting Eqs. (29) and (30) in Eq. (15), the following set of equations is obtained

$$\begin{aligned} \ddot{\boldsymbol{\psi}} = {} & H_{\psi\psi}(-C_{\psi\psi}\dot{\boldsymbol{\psi}} - \varepsilon^2 C_{\psi q}\overline{K}_{qq}^{-1}\dot{z} - K_{H_\psi} + \boldsymbol{\tau}) \\ & + H_{\psi q}(-C_{q\psi}\dot{\boldsymbol{\psi}} - \varepsilon^2 C_{qq}\overline{K}_{qq}^{-1}\dot{z} - z - K_{H_q} - \varepsilon\overline{K}_{p_{elastelect_a}}\boldsymbol{\nu}_a) \end{aligned} \tag{31}$$

and

$$\begin{aligned} \varepsilon^2\ddot{z} = {} & \overline{K}_{qq}H_{q\psi}(-C_{\psi\psi}\dot{\boldsymbol{\psi}} - \varepsilon^2 C_{\psi q}\overline{K}_{qq}^{-1}\dot{z} - K_{H_\psi} + \boldsymbol{\tau}) \\ & + \overline{K}_{qq}H_{qq}(-C_{q\psi}\dot{\boldsymbol{\psi}} - \varepsilon^2 C_{qq}\overline{K}_{qq}^{-1}\dot{z} - z - K_{H_q} - \varepsilon\overline{K}_{p_{elastelect_a}}\boldsymbol{\nu}_a) \end{aligned} \tag{32}$$

where $H = M^{-1}$. The model of the slow subsystem, by considering $\varepsilon = 0$ and solving for z in Eq. (32), is obtained

$$z_s = H_{qq}^{-1}H_{q\psi}(-C_{\psi\psi}\dot{\boldsymbol{\psi}}_s - K_{H_\psi} + \boldsymbol{\tau}_s) - C_{q\psi}\dot{\boldsymbol{\psi}}_s - K_{H_q} \tag{33}$$

herein, subscript *s* indicates that the system is considered in the slow time scale. Substituting Eq. (33) in (31) yields

$$\begin{aligned} \ddot{\boldsymbol{\psi}}_s &= (H_{\psi\psi} - H_{\psi q}H_{qq}^{-1}H_{q\psi})(-C_{\psi\psi}\dot{\boldsymbol{\psi}}_s - K_{H_\psi} + \boldsymbol{\tau}_s) \\ &= M_{\psi\psi}^{-1}(-C_{\psi\psi}\dot{\boldsymbol{\psi}}_s - K_{H_\psi} + \boldsymbol{\tau}_s) \end{aligned} \tag{34}$$

By choosing $\xi = t/\varepsilon$, introducing $z_f = z - z_s$ and considering both the slow variables as constant in fast time scale and the terms of $O(\varepsilon^2)$ and higher equal to zero, the fast subsystems can be obtained as

$$\begin{aligned}\frac{d^2}{d\xi^2} z_f &= -\varepsilon \overline{K}_{qq} (H_{q\psi} C_{\psi q} \overline{K}_{qq}^{-1} + H_{qq} C_{qq} \overline{K}_{qq}^{-1}) \frac{d}{d\xi} z_f - \overline{K}_{qq} H_{qq} z_f \\ &\quad - \varepsilon \overline{K}_{qq} H_{qq} \overline{K}_{p_{elastelect_a}} \boldsymbol{v}_a\end{aligned} \tag{35}$$

b) Adaptive inverse dynamics control for the slow subsystem

Controllers that can handle regulation and tracking problems without the need for knowledge of the process parameters are by themselves an appealing procedure. Such controller schemes belong to the class of adaptive control. Equation (15) is linear in dynamic parameters and can be written as [26]:

$$M_{\psi\psi} \ddot{\psi} + C \dot{\psi} + K_{H_\psi} = Y \boldsymbol{\rho} \tag{36}$$

where Y is known as the regression matrix and $\boldsymbol{\rho}$ is the vector of parameters of the system. The control input can be determined by:

$$\boldsymbol{\tau} = \hat{M}_{\psi\psi} (\ddot{\psi}_d - K_D \dot{\tilde{\psi}} - K_P \tilde{\psi}) + \hat{C}_{\psi\psi} \dot{\psi} + \hat{K}_{H\psi} \tag{37}$$

We assume here that $\hat{M}_{\psi\psi}$, $\hat{C}_{\psi\psi}$ and $\hat{K}_{H_\psi}$ have the same functional form as $M_{\psi\psi}$, $C_{\psi\psi}$ and K_{H_ψ} with estimated parameters $\hat{\boldsymbol{\rho}}$. With respect to (36) we can write the following equation:

$$\boldsymbol{\tau} = Y \hat{\boldsymbol{\rho}} \tag{38}$$

Substituting (36) into the dynamics of the system gives the following closed-loop error equation

$$\hat{M}_{\psi\psi} (\ddot{\tilde{\psi}} + K_D \dot{\tilde{\psi}} + K_P \tilde{\psi}) = Y \tilde{\boldsymbol{\rho}} \tag{39}$$

where $(\tilde{\cdot}) = (\cdot) - (\cdot)_{desired}$ and

$$Y \tilde{\boldsymbol{\rho}} = (\hat{M}_{\psi\psi} - M_{\psi\psi}) \ddot{\psi} + (\hat{C}_{\psi\psi} - C_{\psi\psi}) \dot{\psi} + (\hat{K}_{H_\psi} - K_{H_\psi}) \tag{40}$$

The error equation in (39) can be rewritten as

$$\ddot{\tilde{\psi}} + K_D \dot{\tilde{\psi}} + K_P \tilde{\psi} = \hat{M}_{\psi\psi}{}^{-1} Y \tilde{\boldsymbol{\rho}} = \overline{\Phi} \tilde{\boldsymbol{\rho}} \tag{41}$$

This equation can be cast in state space form by choosing $\xi_1 = \tilde{\psi}$, $\xi_2 = \dot{\tilde{\psi}}$, $\xi = (\xi_1^T \ \ \xi_2^T)^T$, i.e.

$$\dot{\zeta} = A\zeta + B\overline{\Phi} \tilde{\boldsymbol{\rho}} \tag{42}$$

with

$$A = \begin{bmatrix} 0 & I \\ -K_P & -K_D \end{bmatrix}, \ B = \begin{bmatrix} 0 \\ I \end{bmatrix} \tag{43}$$

with choosing the Lyapunov function candidate

$$V = \xi^T P\xi + \tilde{\rho}^T \Gamma \tilde{\rho} \tag{44}$$

where P is the unique symmetric positive definite solution to the equation $A^T P + PA = -Q$, for a given symmetric positive definite matrix Q. Taking the time derivative of V gives:

$$\dot{V} = -\xi^T Q\xi + 2\tilde{\rho}^T (\overline{\Phi}^T B^T P\zeta + \Gamma\hat{\rho}) \tag{45}$$

Choosing the update law as

$$\dot{\hat{\rho}} = -\Gamma^{-1}\overline{\Phi}^T B^T P\zeta \tag{46}$$

Equation (45) is reduced to the following form:

$$\dot{V} = -\zeta^T Q\zeta \tag{47}$$

It can be shown that $\zeta \in L_2 \cap L_\infty$, $\hat{\rho} \in L_\infty$, and then the control input τ in (37) is bounded. It follows that $\ddot{\psi} \in L_\infty$ so that $\dot{\xi} \in L_\infty$. Then ζ is uniformly continuous and, since $\xi \in L_2$, it can be concluded that ζ asymptotically converges to zero.

c) Controller design for the fast subsystem

The voltage applying to the piezoelectric actuators is proposed as:

$$\boldsymbol{v}_a = -K_d \dot{\boldsymbol{v}}_s - K_P \boldsymbol{v}_s \tag{48}$$

where K_d and K_P are two positive definite matrices. In order to investigate the stability of the system the Lyapunov approach is used and the following Lyapunov candidate is determined

$$V_{Lyapunov_f} = \frac{1}{2}\dot{\mathbf{q}}_f^T H_{qq}^{-1}\dot{\mathbf{q}}_f + \frac{1}{2}\mathbf{q}_f^T K_{qq}\mathrm{q}_f + \frac{1}{2}K_q \mathbf{q}_f^T K_{p_{elastelect_a}} K_{p_{elastelect_a}}^T \mathbf{q}_f \tag{49}$$

where K_q is a positive definite matrix. Equation (35) can be rewritten as follows:

$$H_{qq}^{-1}\ddot{\mathbf{q}}_f + (H_{qq}^{-1}H_{q\psi}C_{\psi q} + C_{qq})\dot{\mathbf{q}}_f + K_{qq}\mathbf{q}_f = -K_{p_{elastelect_a}}\boldsymbol{v}_a \tag{50}$$

Because the piezoelectric parameters are very small negative values [28], and with respect to Eq. (26), we can write:

$$K_{p_{elect}}^{-1} K_{p_{elastelect_s}}^T = -\mu K_{p_{elastelect_a}}^T = O(1/\varepsilon^2) \tag{51}$$

where μ is a positive scalar. Since the slow variables are considered constant in fast time scale, $\dot{H}_{qq}^{-1} = 0$. By substituting $H_{qq}^{-1}\ddot{\mathbf{q}}_f$ from Eq. (50) and knowing the fact that $\dot{H}_{qq}^{-1} = 0$, the time derivative of Eq. (49) can be written as:

$$\dot{V}_{Lyapunov_f} = -\dot{\mathbf{q}}_f^T (H_{qq}^{-1}H_{q\psi}C_{\psi q} + C_{qq})\dot{\mathbf{q}}_f - K_d\mu\dot{\mathbf{q}}_f^T K_{p_{elastelect_a}} K_{p_{elastelect_a}}^T \dot{\mathbf{q}}_f \tag{52}$$

Here, the second term is a negative term and K_d is defined such that $K_d\mu$ components are of order $1/\varepsilon$. Using Eq. (29) and noting the Eq. (51), the above equation can be written as

$$\begin{aligned}\dot{V}_{Lyapunov_f} &= -\varepsilon^4 \dot{z}_f^T \overline{K}_{qq}^{-1}(H_{qq}^{-1}H_{q\psi}C_{\psi q} + C_{qq})\overline{K}_{qq}^{-1}\dot{z}_f \\ &\quad -\varepsilon^3 \dot{z}_f^T \overline{K}_{qq}^{-1} K_{p_{elastelect_a}} K_{p_{elastelect_a}}^T \overline{K}_{qq}^{-1}\dot{z}_f\end{aligned} \tag{53}$$

Since the first term is of the magnitude $O(\varepsilon^4)$, while the second term is of $O(\varepsilon^3)$, the first term can be ignored and by utilizing the Lyapunov theory and the singular perturbation method, the derivative of Lyapunov function is shown to be negative; therefore, the stability of the fast subsystem with the proposed controller is guaranteed.

4. SIMULATION RESULTS AND DISCUSSION

In order to observe the response of the whole system and performance of the hybrid controller, the flexible spacecraft in an orbit is simulated. First, the accuracy and convergence behavior of the solution method are investigated by obtaining the system response for a different number of mode shapes. The solution process is continued until the difference between the two successive solutions reduces to an acceptable error threshold. Based on a number of simulation runs for various cases, we found that three bending modes are sufficient to reach good accuracy.

The parameters of the piezoelectric layers and the flexible appendages are summarized in Table 1. The desired trajectory of the satellite's maneuver is designed to start and finish with constant acceleration and deceleration, respectively, and in the middle a constant velocity is considered.

Table 1. The characteristics of the piezoelectric layers and the flexible appendages 9

Piezoelectric layer	Flexible appendage
Modulus, $E_p = 2\times10^9\ N/m^2$	Modulus, $E = 76\times10^9\ N/m^2$
Piezoelectric constant, $d_p = 22\times10^{-12}\ mV^{-1}$	Length, $L = 5\,m$
Thickness, $t_p = 1mm$	Thickness, $t_a = 8\,mm$
Width, $b = 0.5\ m$	Width, $b = 0.5\ m$
Density, $\rho_p = 1800 kg/m^3$	Density, $\rho = 2840\,kg/m^3$

In simulating process, governing equations of motion of the system, Eq. (15), are considered and the decomposed equations of motion using singular perturbation theory are used only for hybrid control design. The proposed hybrid controller is applied to the system and as demonstrated in Figs. 2 the adaptive inverse dynamics control utilized for the slow subsystem, which is associated with rigid body motion of the flexible spacecraft, shows a good performance in tracking the desired trajectory and the resulting errors are small. In order to demonstrate the capability and usefulness of the piezoelectric actuators, two cases are simulated. First, we consider the case when the controller is used and the voltages are applied to the piezoelectric actuators. Second, to highlight the effects of the piezoelectric layers, the satellite is equipped with a closed loop central system to track the desired trajectory; but this time, without applying the voltages to the piezoelectric actuators. Figures 3-5 show the time histories of three generalized coordinates of the appendage. Figure 6 represents the tip deflection of the appendage. It can be seen that the piezoelectric actuators play an efficient role in suppressing the adverse vibration of the system. The output voltages of the sensors of the appendage are also presented in Figs. 7-9, respectively. Figure 10 shows the voltages applied to piezoelectric actuators bonded to two appendages. These figures illustrate the performance of the adaptive inverse dynamics controller that is applied to the flexible spacecraft moving in an orbit.

We consider three patches of piezoelectric on each appendage as sensors and three piezoelectric layers as actuators. Each appendage has a similar behavior in the maneuver. Therefore only one appendage response is shown.

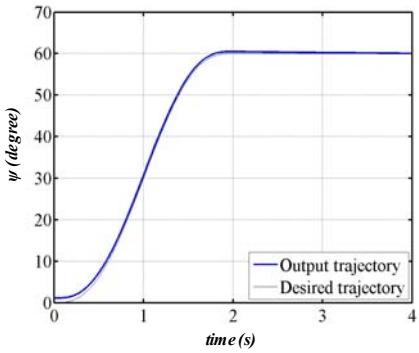

Fig. 2. Trajectory tracking of the angle of rotation of the satellite

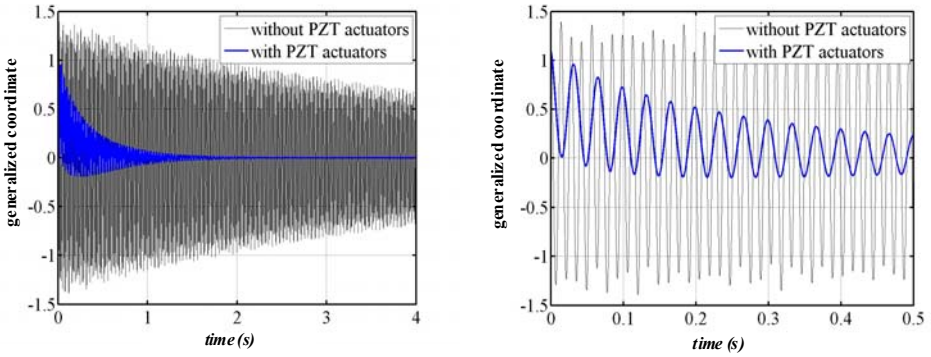

(a) (b)

Fig. 3. Time history of the first generalized coordinate of the appendage: (a) whole domain and (b) magnified from t=0s to 0.5s

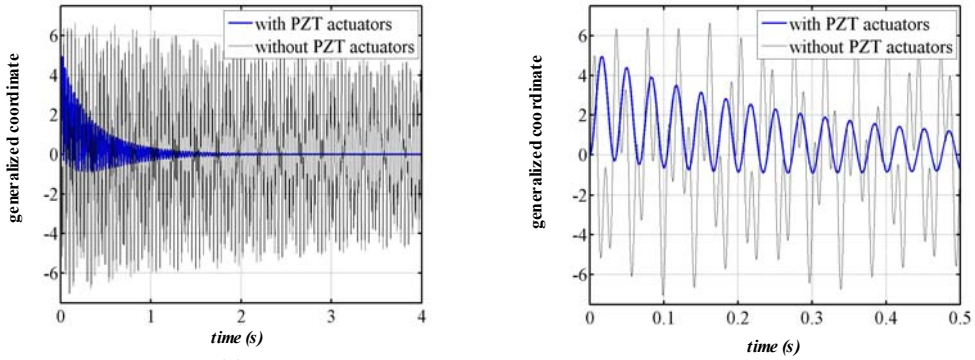

(a) (b)

Fig. 4. Time history of the second generalized coordinate of the appendage: (a) whole domain and (b) magnified from t=0s to 0.5s

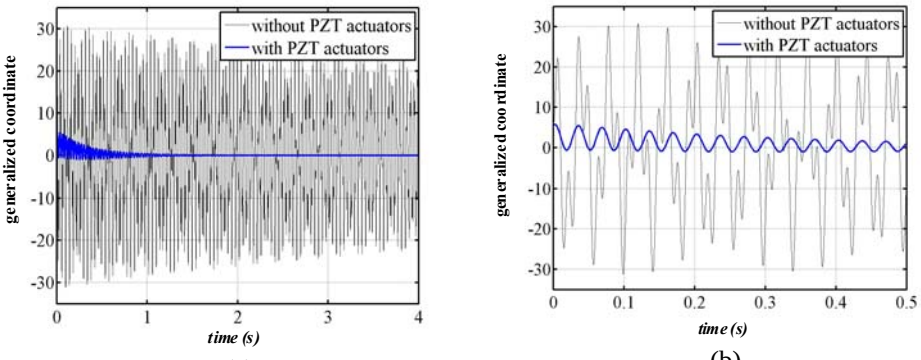

(a) (b)

Fig. 5. Time history of the third generalized coordinate of the appendage: (a) whole domain and (b) magnified from t=0 s to 0.5s

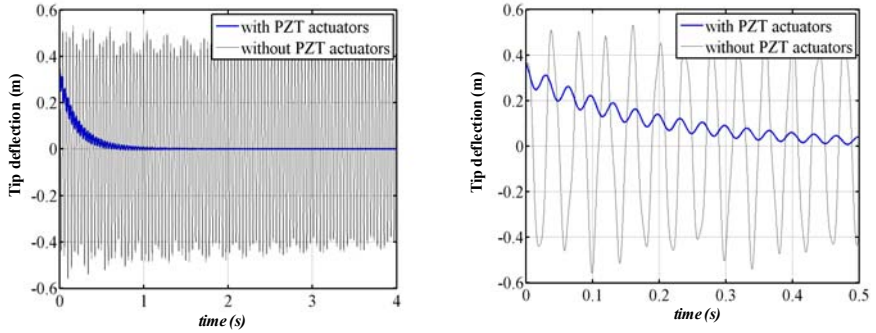

(a) (b)

Fig. 6. Tip deflection of the appendage: (a) whole domain and (b) magnified from t=0 s to 0.5 s

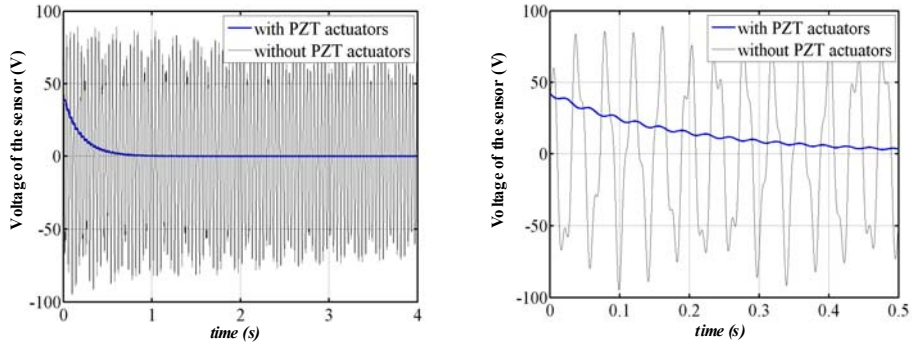

(a) (b)

Fig. 7. Output voltage of first PZT sensor bonded to the appendage: (a) whole domain and (b) magnified from t=0 s to 0.5 s

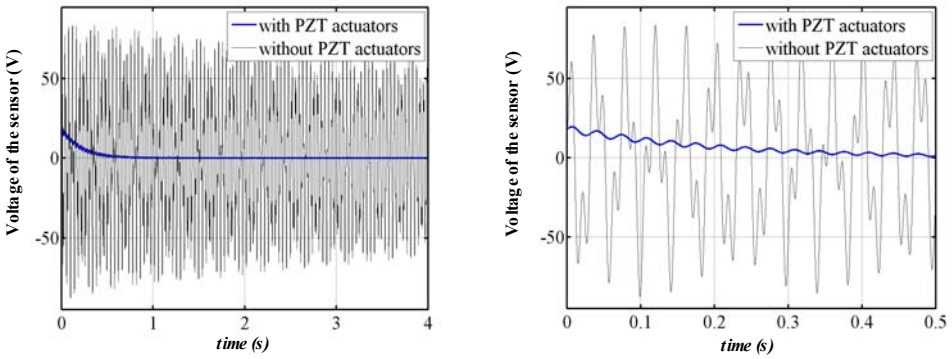

(a) (b)

Fig. 8. Output voltage of second PZT sensor bonded to the appendage: (a) whole domain and (b) magnified from t=0 s to 0.5 s

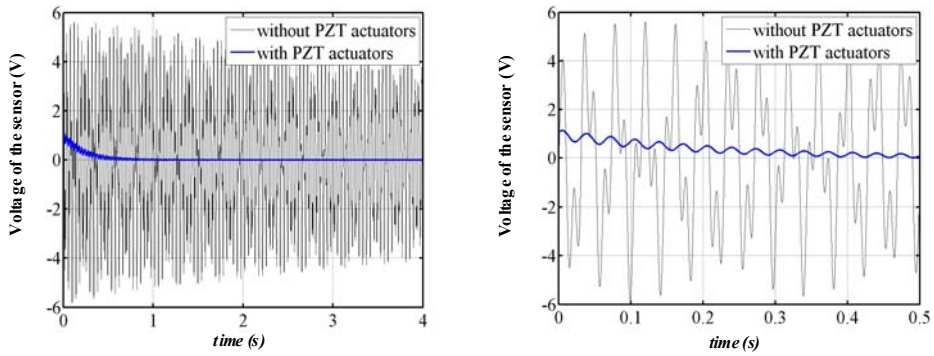

(a) (b)

Fig. 9. Output voltage of third PZT sensor bonded to the appendage: (a) whole domain and (b) magnified from t=0 s to 0.5 s

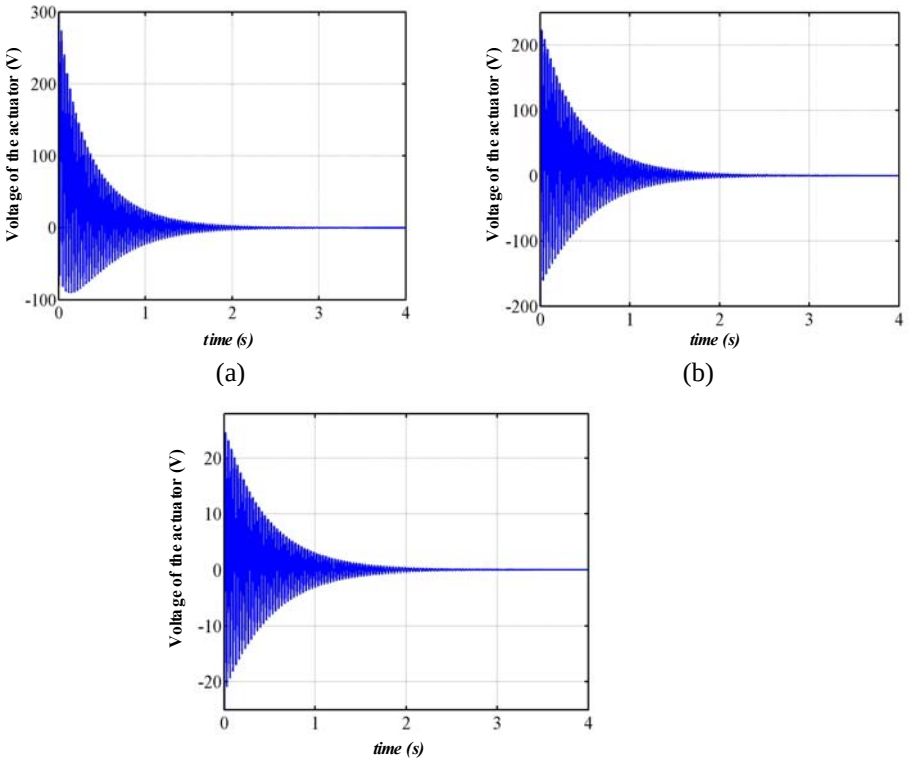

Fig. 10. Applied voltage to PZT actuators bonded to the appendage: (a) first actuator, (b) second actuator and (c) third actuator.

5. CONCLUSION

In this paper a hybrid control scheme was applied to control the maneuver of a flexible satellite in an orbit and suppress the vibrations of the appendages. The piezoelectric layers were attached to the appendages and worked as sensors and actuators. The Lagrange-Rayleigh-Ritz technique is used to derive nonlinear governing equations of motion and no simplification was considered in their derivation. Because of the flexibility and maneuvering in an orbit, the governing equations were coupled and quite complicated. In order to apply the controller, the governing equations of the system were decomposed into slow and fast subsystems using the singular perturbation theory. Then, an adaptive inverse dynamics control for slow and a Lyapunov based controller for the fast subsystem were proposed and developed. The fast and slow subsystems were used only for applying the controller, and in order to simulate the responses of the system the general coupled equations of motion were used. Finally, the system was simulated and the outcomes confirmed the advantages of the hybrid control scheme.

REFERENCES

1. Gennaro, S. D. (2003). Output stabilization of flexible spacecraft with active vibration suppression. *IEEE Transactions on Aerospace and Electronic Systems*, Vol. 39, No. 3, pp. 747-759.
2. Jan, Y. W. & Chiou, J. C. (2003). Minimum-time spacecraft maneuver using sliding-mode control. *Acta Astronautica*, Vol. 54, pp. 69-75.
3. Bang, H., Cho, Y. & Lee, H. (2004). Slewing maneuvering control of flexible spacecraft by output feedback. *Acta Astronautica*, Vol. 55, pp. 903-916.
4. Ge, Sh. S., Lee, T. H., Hong, F. & Goh, Ch. H. (2004). Energy-based robust controller design for flexible spacecraft. *Journal of Control Theory and Applications*, Vol. 2, pp. 27-34.

5. Binglong, C., Xiangdong, L. & Zhen, C. (2010). Exponential time-varying sliding mode control for large angle attitude eigen axis maneuver of rigid spacecraft. *Chinese Journal of Aeronautics*, Vol. 23, pp. 447-453.
6. Hu, Q. (2009). A composite control scheme for attitude maneuvering and elastic mode stabilization of flexible spacecraft with measurable output feedback. *Aerospace Science and Technology Journal*, Vol. 13, pp. 81- 91.
7. Jiang, Y., Hu, Q. & Ma, G. (2010). Adaptive backstepping fault-tolerant control for flexible spacecraft with unknown bounded disturbances and actuator failures. *ISA Transactions*, Vol. 49, pp. 57-69.
8. Erdong, J. & Zhaowei, S. (2010). Passivity-based control for a flexible spacecraft in the presence of disturbances. *International Journal of Non-Linear Mechanics*, Vol. 45, pp. 348–356.
9. Li, Z. & Bainum, P. M. (1994). Vibration control of flexible spacecraft integration a momentum exchange controller and a distributed piezoelectric actuator. *Journal of Sound and Vibration*, Vol. 177, No. 4, pp. 539-553.
10. Hu, Q. & Ma, G. (2006). Spacecraft vibration suppression using variable structure output feedback control and smart materials. *Journal of Vibration and Acoustics*, Vol. 128, pp. 221-230.
11. Hu, Q. & Ma, G. (2006). Variable structure maneuvering control and vibration suppression for flexible spacecraft subject to input nonlinearities. *Smart Materials and Structures*, Vol. 15, pp. 1899- 1911.
12. Hu, Q. (2008). Sliding mode maneuvering control and active vibration damping of three-axis stabilized flexible spacecraft with actuator dynamics. *Nonlinear Dynamics*, Vol. 52, pp. 227- 248.
13. Qiu, Z. C., Wu, H.X. & Zhang, D. (2009). Experimental researches on sliding mode active vibration control of flexible piezoelectric cantilever plate integrated gyroscope. *Journal of Thin-Walled Structures*, Vol. 47, pp. 836–846.
14. Azadi, M., Fazelzadeh, S. A., Eghtesad, M. & Azadi, E. (2011). Vibration suppression and adaptive-robust control of a smart flexible satellite with three axes maneuvering. *Acta Astronautica*, Vol. 69, pp. 307-322.
15. Azadi, M. (2012). Maneuver control and vibration suppression of a smart flexible satellite using robust passivity based control. *Advanced Materials Research*, Vol. 488, p. 1803.
16. Singh, S. N. & Zhang, R. (2004). Adaptive output feedback control of spacecraft with flexible appendages by modeling error compensation. *Acta Astronautica*, Vol. 54, pp. 229- 243.
17. Hui, L., Junfeng, L. & Baoyin, H. (2006). Sliding mode control for low-thrust Earth-orbiting spacecraft formation maneuvering. *Aerospace Science and Technology*, Vol. 10, pp. 636-643.
18. Maganti, G. B. & Singh, S. N. (2007). Simplified adaptive control of an orbiting flexible spacecraft. *Acta Astronautica*, Vol. 61, pp. 575-589.
19. Dong, C., Xu, L., Chen, Y. & Wang, Q. (2009). Networked flexible spacecraft attitude maneuver based on adaptive fuzzy sliding mode control. *Acta Astronautica Journal*, Vol. 65, pp. 1561–1570.
20. Hu, Q., Li, B. & Zhang, Y. (2013). Robust attitude control design for spacecraft under assigned velocity and control constraints. *ISA Transactions*, http://dx.doi.org/10.1016/j.isatra.2013.03.003i
21. Meirovitch, L. (1997). Principles and techniques of vibrations. Prentice-Hall, New Jersey.
22. Fazelzadeh, S. A., Eghtesad, M. & Azadi, M. (2010). Buckling and flutter of a column enhanced by piezoelectric layers and lumped mass under a follower force. *International Journal of Structural Stability and Dynamics*, Vol. 10, pp. 1083-1097.
23. Crawley, E. F. & de Luis, J. (1987). Use of piezoelectric actuators as elements of intelligent structures. *AIAA Journal*, Vol. 25, pp. 1373–1385.
24. Clark, R. L., William, R. S. & Gibbs, G. P. (1998). *Adaptive structures: Dynamics and control*. John Wily.
25. Baruh, H. (1999). Analytical dynamics. *WCB/McGraw-Hill, Boston.*
26. Canudas, C., Siciliano, B. & Bastin, G. (1997). *Theory of robot control*. Springer, New York.
27. Kokotovic, P., Khalil, H. K. & O'Reilly, J. (1999). *Singular perturbation methods in control: Analysis and design*. SIAM, Philadelphia.
28. Necsulescu, D. S. (2001). *Mechatronics*. Prentice Hall.